




Dislocation-controlled microscopic mechanical phenomena in single crystal silicon under bending stress at room temperature

Hiroshi Yamaguchi¹, Junichi Tatami^{1,2,*} , Tsukaho Yahagi², Hiromi Nakano³, Motoyuki Iijima^{1,2}, Takuma Takahashi², and Toshiyuki Kondo²

¹Yokohama National University, 79-7 Tokiwadai, Hodogayaku, Yokohama, Kanagawa 240-8501, Japan

²Kanagawa Institute of Industrial Science and Technology, 705-1 Shimoimaizumi, Ebina, Kanagawa 243-0435, Japan

³Toyohashi University of Technology, 1-1 Hibarigaoka, Tempaku, Toyohashi, Aichi 441-8580, Japan

Received: 19 September 2019

Accepted: 28 January 2020

Published online:

11 March 2020

© Springer Science+Business Media, LLC, part of Springer Nature 2020

ABSTRACT

Silicon is widely used within energy, electro-mechanical, environmental devices by nanostructural control. As silicon parts constitute structural components whose size is ever decreasing, it is critical to understand the mechanical properties of single crystal silicon from precise measurements of load and displacement using microscopic sample in sub-micron and macroscopic scales. Here, the mechanical properties of single crystal silicon were precisely evaluated by bending tests at room temperature using microcantilever beam specimens having a several micron size. The microcantilever beam specimens were prepared using a focused ion beam technique, followed by loading the tip of the specimens. The smaller specimens deformed nonlinearly and then fractured. The unloaded specimen after nonlinear deformation showed permanent strain and many dislocations close to the region where high tensile stress was applied. This means that the nonlinear stress–strain relationship in the very high bending stress is determined by plastic deformation controlled by dislocation despite occurring at room temperature. The bending strength increased with a decrease in specimen size, and the smallest specimens had close to ideal strength. The size of the region where the dislocations accumulated in high density corresponded to the flaw size estimated from the fracture mechanics. This means that the bending strength of the microcantilever beam specimens of silicon is dominated by newly generated defects resulting from dislocations; in other words, the size effect of bending strength of silicon at the micrometer scale is controlled by the accumulation of newly formed dislocations because the dense dislocation region should be lower in a smaller-sized specimen.

Address correspondence to E-mail: tatami-junichi-xv@ynu.ac.jp

Introduction

Silicon, a widely known semiconductor material, is often used in various devices with nano- to macrostructures such as solar power generation [1], lithium-ion batteries [2, 3], photovoltaics [4], and microelectromechanical systems devices [5–12]. Such devices require both excellent functionality and highly reliable mechanical properties as they are a part of structural components. It is well known that bulk single crystal silicon material typically fractures in a brittle manner at room temperature [13, 14]. The bending and tensile strength of larger specimens of such brittle materials are controlled by the size of defects according to the theory of fracture mechanics. Thus, a reduction in the overall sample size of a sample can result in an increase in both the bending and tensile strength, owing to a decrease in the size of the fracture origin [15]. It is critical to evaluate and form comparisons of mechanical properties using specimens of the same scale of the resulting device to increase the mechanical reliability of such microscopic devices. Additionally, mechanical properties specific to the microscopic scale may appear, owing to the high-stress field.

The mechanical properties of small single crystal silicon specimens have been evaluated using various techniques [12, 16–41]. Micropillar compression and indentation tests have been carried out using a diamond indenter [16, 17]. The compressive strength of brittle materials is usually measured to be higher than either their bending or tensile strength. These materials typically plastically deform as a result of these compression and indentation tests when the compressive strength exceeds the yield stress resulting from the generation and movement of dislocations. Two types of dislocation may occur within diamond structured single crystal silicon: shuffle set dislocation and glide set dislocation. When single crystal silicon is compressed at 400 °C or higher, the glide set dislocation is predominant active dislocation mode [18–21]. At lower temperatures, however, indents and scratches result in shuffle set dislocation, a complete dislocation [22, 23]. When compressed at room temperature, samples display a combination of dislocation types as the dominant shuffle set dislocation transforms to glide set dislocation [24–26]. Similar to temperature effects, it has been reported that dislocations generated under compressive stress

affect the mechanical properties of silicon [27]. Additionally, the plastic deformation of single crystal silicon has been observed in both tensile and bending tests at 400 °C [28, 29] and by grinding tests [30], respectively. The evaluation of bending and tensile strength has been carried out with specimens as small as several μm [12, 28, 31–41]. The results obtained by these studies revealed that small specimen can exhibit extremely high tensile and bending strength amounting to several GPa. Furthermore, the size effects of tensile strength for single crystal silicon have been reported [12]. In the case of small specimens, similar high strength values have also been reported for other materials [42–49].

Although the mechanical properties of micro single crystal silicon have been evaluated through various methods, as mentioned above, there still exist many aspects and characteristics that have not been examined. The same phenomena likely occur under both tensile and compressive stress. However, plastic deformation has been observed only under compression tests at room temperature. As the tensile strength and bending strength of small specimen are very high, amounting to several GPa, single crystal silicon is expected to plastically deform at room temperature when subjected to either tensile or bending stress; this active deformation mode is due to the generation and movement of transposition. Moreover, it may be difficult to specify portions of a specimen that has undergone plastic deformation because the measurement of tensile stress is performed by applying force uniformly to the entire specimen. Due to a high degree of localization in the higher tensile stress region during a bending test, one may easily observe possible dislocations. Defects that are expected to control the strength and its size effect in a microscopic specimen have not been sufficiently clarified for either bending or tensile modes. Furthermore, previous studies yet to resolve these issues, owing either to improperly measured displacements or observing specimens using TEM only after applying stress.

Herein, the yield phenomenon and strength of small single crystal silicon specimens under bending stress were successfully evaluated at room temperature by subjecting microcantilever beam specimens prepared using a focused ion beam technique (FIB) to a bending test. The relationship between the applied load and the displacement of the loading point was evaluated through observations made by scanning

electron microscopy (SEM) observation of the fracture surface and TEM observations of pre-fracture specimens after applications of high bending stress were carried out.

Experimental

Microcantilever beam specimens were prepared on the surface of single crystal silicon via FIB (XVision 200 TB, SII NanoTechnology Inc., Tokyo, Japan). The crystal orientation in the longitudinal direction of the specimens was $\langle 1\ 1\ 0 \rangle$, and the crystal plain at the top of the specimen was $(1\ 0\ 0)$. The surface of the single crystal silicon used in this study underwent chemical mechanical polishing before machining the microcantilever beam specimens. The dislocation density—as measured by counting the number of etch pits—was $2.6 \times 10^3\text{ cm}^{-2}$. A microcantilever beam specimen was fabricated using an acceleration voltage of 30 kV. As presented in Table 1, three types of specimens were prepared with various heights, widths, and lengths. As a representative example, the MEDIUM specimen, prepared using the focused ion beam technique, is shown in Fig. 1. The microcantilever beam specimens were fractured by loading applied at a load point distance presented in Table 1 from the fixed end of the beam. The bending tests were carried out on the microcantilever beam specimens using a nanoindenter (TI Premier, Bruker, USA). The load was applied to the specimens using a cube corner-type diamond indenter with an approach rate of 30 nm s^{-1} . For SMALL samples only, the loading rate was set to 15 nm s^{-1} . The relationship

between the load and displacement was obtained through a bending test conducted on the specimens. Some of the MEDIUM specimens were tested to unload the stress before the fracture occurred.

The mechanical properties (stress, strain, and Young’s modulus) of the specimens were calculated from the load and displacement via beam theory-based calculations. According to beam theory, the mechanical properties can be calculated using the following equations:

$$\sigma = \frac{PLa}{I} \tag{1}$$

$$\varepsilon = \frac{3da}{L^2} \tag{2}$$

$$E = \frac{\sigma}{\varepsilon} = \frac{PL^3}{3dI} \tag{3}$$

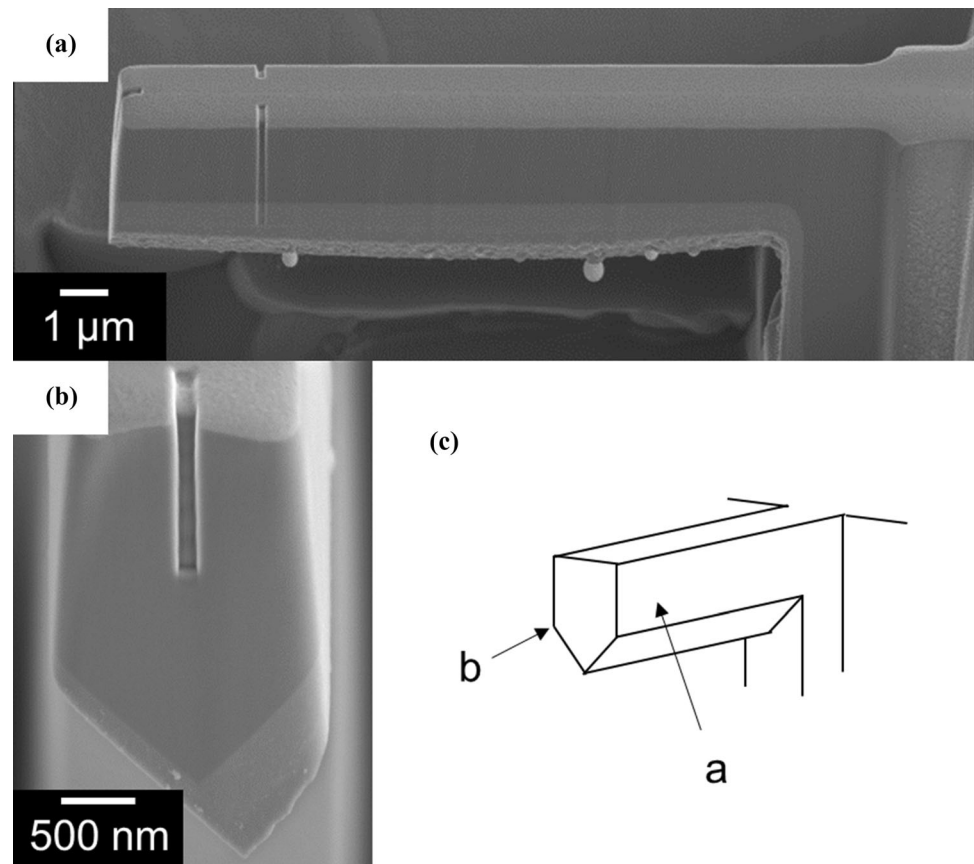
where σ is the bending stress, ε is the strain, E is Young’s modulus, P is the applied load, L is the load point distance, a is the distance from the neutral plane, I is the second moment of area calculated for a pentagonal cross section, and d is the displacement at the loading point.

The highest bending stress is applied at the surface of the fixed end of the microcantilever beam specimen. The yield phenomenon, caused by the dislocation activity, should occur near the region displaying the highest bending stress in the microcantilever beam specimen. Thin samples were prepared using the FIB technique using material from the near and far positions of the surface and from the end part of the MEDIUM specimen after loading before fracture. These samples were observed using a TEM (JEM-

Table 1 Size of microcantilever beam specimens and measured mechanical properties of single crystal silicon samples

Specimens	Small	Medium	Large
Geometry			
Thickness (μm)	0.5	1.5	3.6
Height (μm)	1.2	2.5	6.6
Length (μm)	4.9	15.8	22.4
Displacement to loading point (μm)	3.9 ± 0.1	10.3 ± 0.4	19.5 ± 0.2
Mechanical properties			
Young’s modulus (GPa)	171 ± 31	175 ± 10	143 ± 9
Yield stress (GPa)	4.1 ± 1.0	4.0 ± 0.6	–
Peierls stress (GPa)	1.7 ± 0.4	1.6 ± 0.2	–
Bending strength (GPa)	14.2 ± 1.4	9.0 ± 1.4	4.1 ± 0.4
Crack length $2c$ (nm)			
(Penny-shaped crack)	8.9 ± 1.9	25.3 ± 13.7	105.6 ± 19.4
(Straight through crack)	3.6 ± 0.8	10.3 ± 5.5	42.8 ± 7.9

Figure 1 Microcantilever beam specimens prepared using focused ion beam technique: **a** side view; **b** front view; and **c** schematic illustration and direction of view.



2100F (JEOL Co., Ltd., Tokyo, Japan)) operating at 200 kV.

The fracture origin for microcantilever beam specimens was evaluated by SEM (FE-SEM, SU8010, Hitachi High-Technologies, Tokyo, Japan) observations, while operating at 5 kV. According to linear elastic fracture mechanics, the strength is related to the fracture toughness and the crack geometry through the following equation:

$$\sigma_f = \frac{K_{IC}}{Y\sqrt{\pi c}} \quad (4)$$

where σ_f is the bending strength, Y is a function of crack shape, c is the crack length, and K_{IC} is the fracture toughness. The fracture toughness, K_{IC} , of the single crystal silicon used in this study was measured using single-edge notched microcantilever beam specimens in the same way as previous studies [43]. To prepare the microcantilever beam specimens used in this study, surface geometry observations were made using a scanning probe microscope (SPM, SPA-400, Hitachi High-Technologies, Tokyo, Japan) of the polished surfaces. The observation was performed in dynamic force mode (DFM) using a

microcantilever (SI-DF20, back AL coating, Hitachi High-Technologies, Tokyo, Japan). The surface profile of silicon substrate samples (1- μ m squares) was measured; the difference between the highest and lowest points was calculated and treated as the maximum height toughness.

Results and discussion

Young's modulus for single crystal silicon microcantilever beam specimens

The measured depths of indentations generated during the bending test on the microcantilever beam specimen includes both the depth of the indent itself and the displacement of the microcantilever beam specimen at the loading point. Therefore, displacement at the loading point of a microcantilever beam specimen was calculated by then subtracting the indentation depth measured when the indentation test was carried out on a flat surface of the single crystal silicon using the cube corner-type diamond indenter at the same load; see Fig. 2, and note that

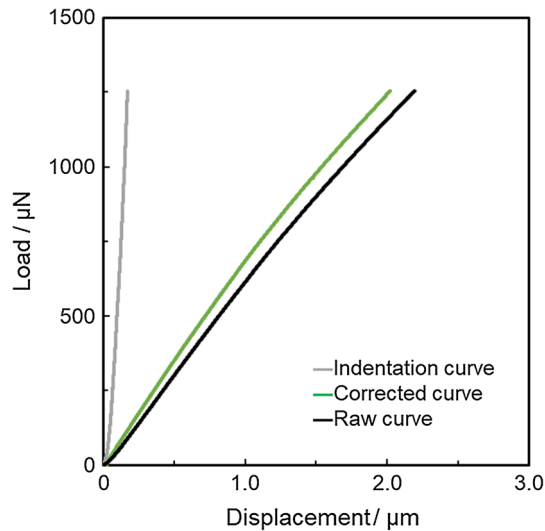


Figure 2 The corrected load–displacement curve is obtained by subtracting the indentation depth from the raw data.

this methodology has been adopted from a previous study [50]. The load–displacement curves—obtained by fracture tests conducted on microcantilever beam specimens with different sizes—are shown in Fig. 3. For LARGE specimens, the relationship between load and displacement was linear, then fracture occurred. On the other hand, the above relationship became slightly nonlinear as the load increased for both MEDIUM and SMALL specimens. Herein, the stress and the strain were calculated from the load and displacement using the aforementioned beam theory equations; this method was selected because of the nonlinearity before fracture and the failure displacement was small.

Because the Young's modulus is a material constant, the validity of our bending test can be determined by the agreement of the measured Young's modulus with the theoretical value; largely, the disagreement comes from an inappropriate second moment of area, which is related to the sample geometry. Furthermore, the cross section of the microcantilever beam specimen was pentagonal, therefore it is difficult to prepare specimens with perfectly symmetrical cross section. If the cross section is too asymmetric, an invalid Young's modulus will be obtained as the specimen undergoes twisting during bending tests. The relationship between cross-sectional asymmetry (skewness) and the Young's modulus is shown in Fig. S1. Figure S1 shows that the Young's modulus can be measured properly for skewness values less than 0.16. Herein, samples

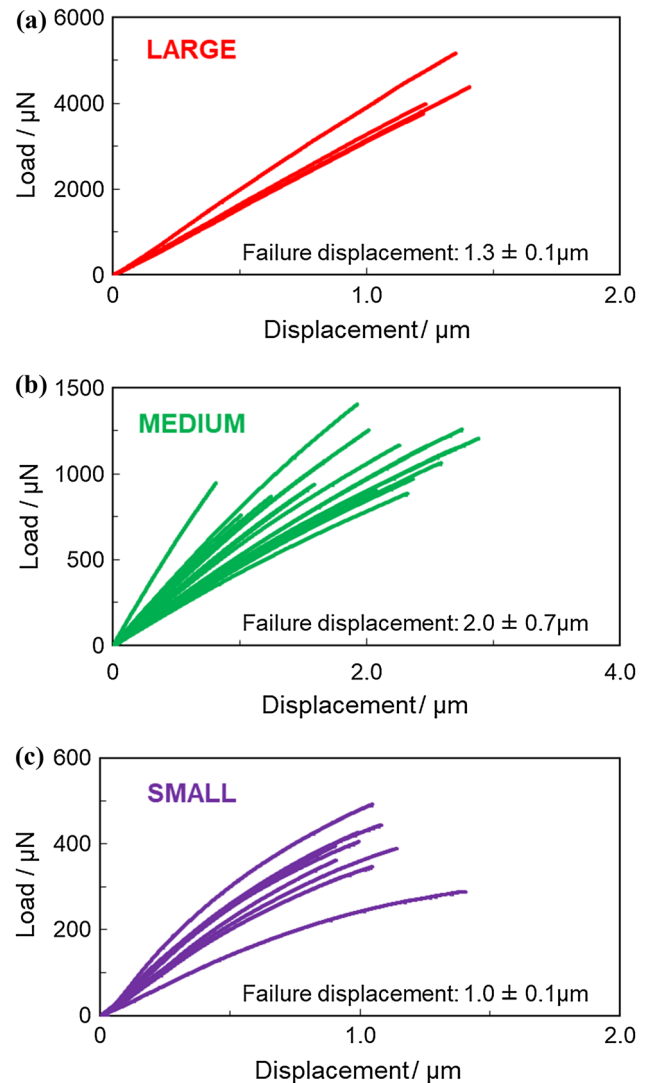


Figure 3 Load–displacement curves measured using microcantilever beam specimens: **a** LARGE, **b** MEDIUM, and **c** SMALL.

displaying a cross-sectional skewness smaller than 0.16 were used to estimate the mechanical properties of single crystal silicon by beam theory.

The stress–strain curves produced using this approach are provided in Fig. 4. The Young's modulus—as calculated from the slope of the region the stress and strain had a linear relationship—are listed in Table 1. The measured Young's moduli for microcantilever beam specimens of various sizes roughly agreed with the ideal value from first-principle calculations [51]. These results confirmed that the microcantilever method achieved approximately valid results.

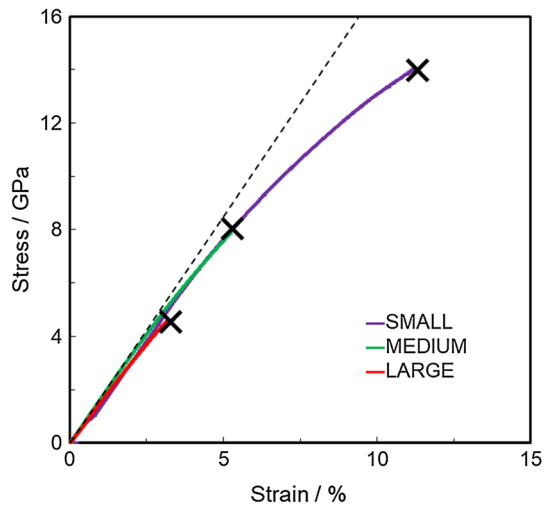


Figure 4 Stress–strain curves measured using microcantilever beam specimens with various sizes. The broken line is the Young’s modulus calculated from first-principle calculation [51].

Yield phenomenon for single crystal silicon

We shall now discuss results related to the stress–strain curves shown in Fig. 4. Herein, we found that the relationship between the stress and strain was linear for the LARGE specimen. Additionally, brittle fracture was observed, similar to the general case defined for bulk single crystal silicon. On the contrary, the stress increased linearly with the strain in the low-stress regime, yet became nonlinear with increasing stress for MEDIUM and SMALL specimens. To investigate the nonlinear relationship of the stress–strain curves, an unloading test for the MEDIUM specimen was performed before fracture, as shown in Fig. 5. Hysteresis was observed in the stress–strain curve during the unloading test conducted on the MEDIUM specimen; this confirms that the specimen subjected to the unloading test displayed permanent strain effects resulting from plastic deformation. Therefore, the nonlinear stress–strain relationship resulted from plastic deformations in the MEDIUM and SMALL specimens.

TEM observations were carried out to clarify the origin of the observed plastic deformations in the microcantilever beam specimens after bending was produced by the single crystal silicon. The TEM images of the unloaded MEDIUM specimen taken from the [110] zone axis are shown in Fig. 6. The maximum applied tensile stress of this specimen was 7 GPa. The observed point is the upper part of the fixed end of the beam, where the highest bending

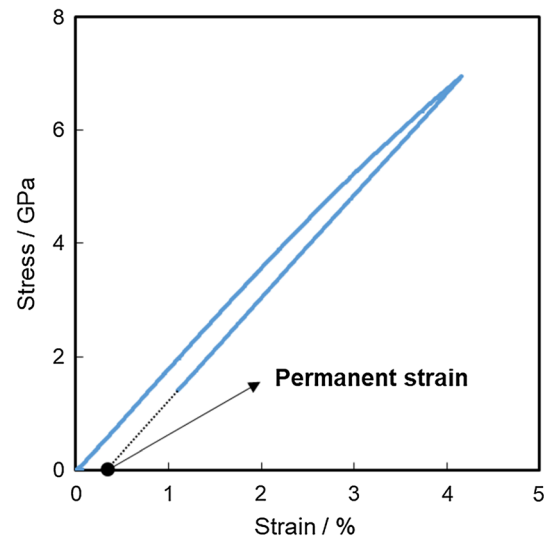
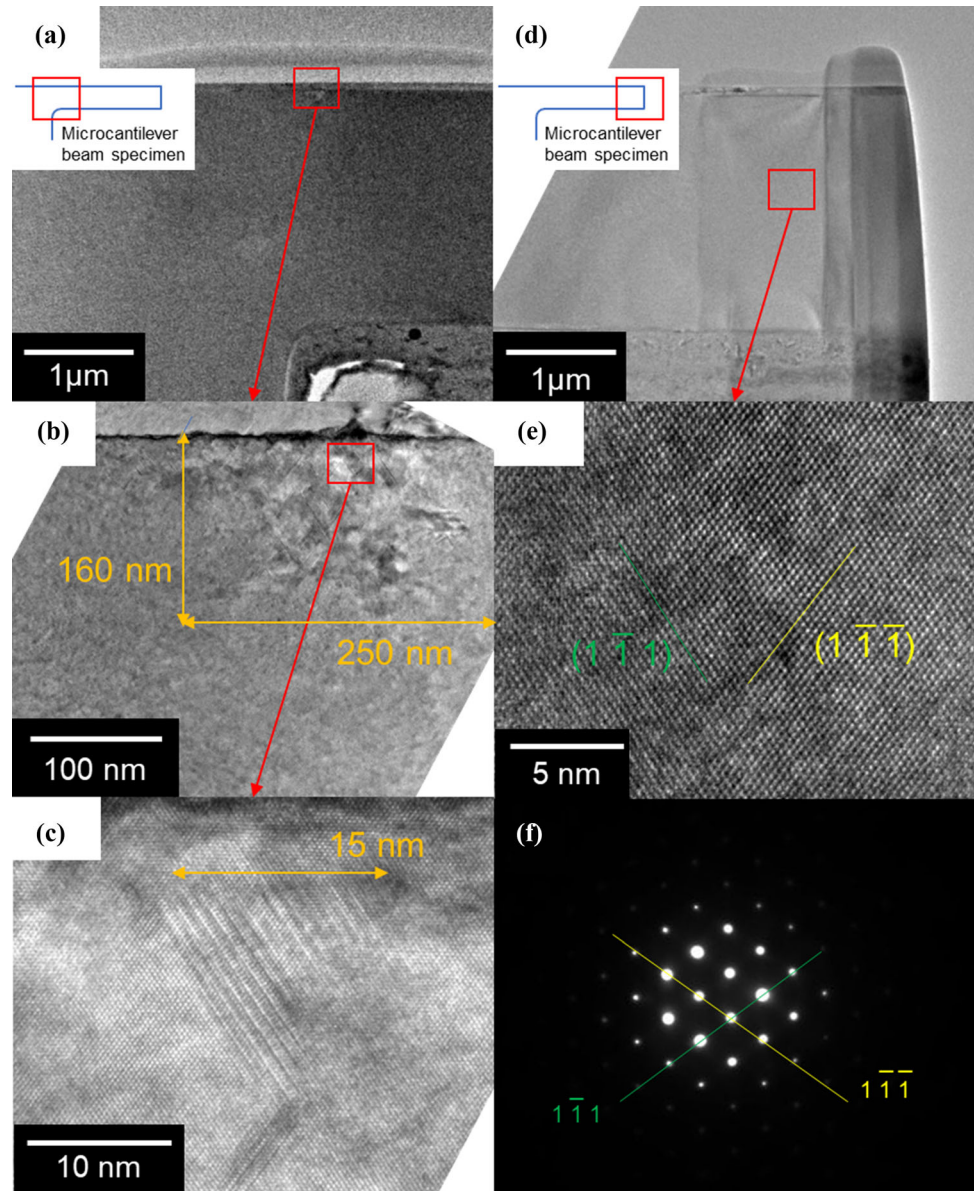


Figure 5 Stress–strain curve of unloading before fracture measured using MEDIUM microcantilever beam specimen.

stress was likely applied. In Fig. 6b, dislocations were observed to be concentrated in the area where higher bending stresses were applied. The size of this region was approximately 200 nm. According to the TEM images provided in Fig. 6d, e, no damage was observed resulting from Ga ion irradiation on the surface of the microcantilever beam specimen, indicating that FIB damage has a marginal effect on critical flaw size and bending strength. The initial dislocation density was very low, with a value of $2.6 \times 10^3 \text{ cm}^{-2}$. Observation indicates dislocations in the low-stress region of the microcantilever beam specimens as shown in Fig. 6d, e, supportive of a low dislocation density. Generally, line contrast due to dislocation is needed to estimate the dislocation density. As shown in Fig. 6b, c, dislocations aggregated in a narrow area; observation of dislocations in these areas require high magnification imaging by weak beam TEM. In such a case, the imaging of dislocation contrast under high magnification is difficult when drifting occurs and/or the dislocation vector is slightly different. Therefore, a quantitative analysis regarding changes in the dislocation density was not carried out in this study.

The results of our crystal structure analysis based on the enlarged view of Fig. 6c are shown in Fig. 7a. Note that not all circles within the figure are representative of Si atoms. Dislocations were observed along the (1 1 1) plane, which is the slip plane of the diamond structure. The diamond structure—the crystal structure of single crystal silicon—has a face-

Figure 6 TEM images of the unloaded MEDIUM specimen: **a** image near the fixed end of the beam; **b** enlarged image of (a); **c** enlarged image of (b); **d** image near the tip of the beam; **e** enlarged image of (d); and **f** diffraction pattern.

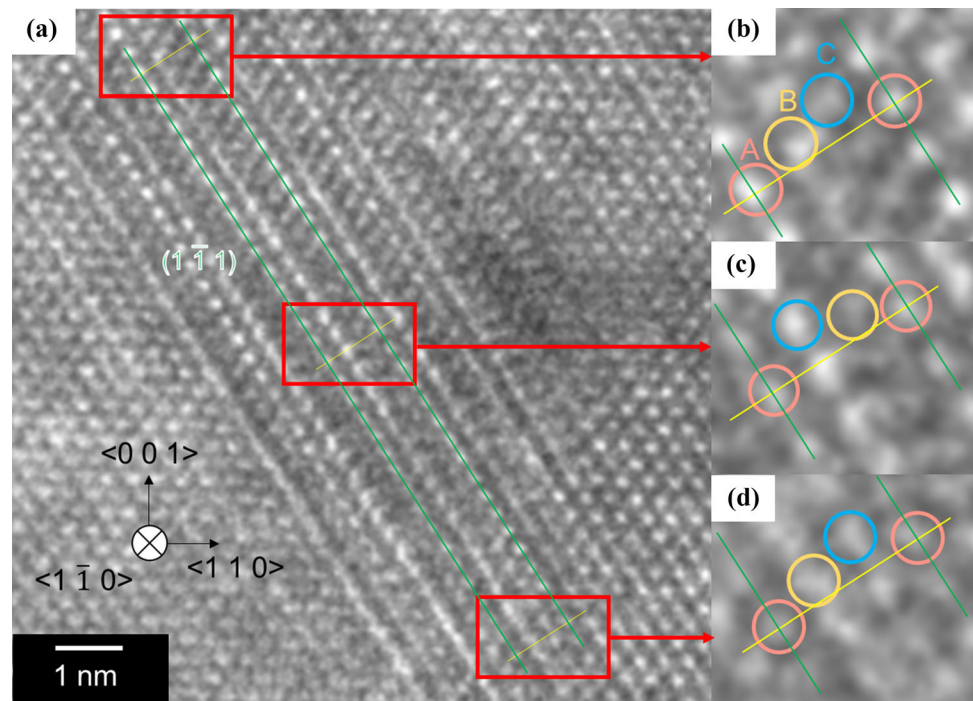


centered cubic Bravais lattice, and a structure consisting of three ABCABC cycles. Figure 7b–d shows enlarged views of Fig. 7a. In Fig. 7b, d, the atoms are regularly stacked in the ABCA form. Conversely, in Fig. 7c, the regular stacked condition collapsed and changed to ACBA in the middle position. Although bright spots in lattice images do not always indicate each atom, it was still clear that the stacking structure was irregular in the region shown in Fig. 7c. Discontinuities in this periodic structure likely result from dislocation, which is considered to have been caused by twinning deformation and stacking faults. The twin plane of the diamond structure was (1 1 1), whereas the twinning deformation appears with the

A plane as the twin plane. If the region observed in Fig. 7c was indeed a twinning deformation, it is impossible to explain why only one layer—squeezed in between the A planes—appeared bright.

The structure shown in Fig. 7c can also be attributed to stacking faults. When a stacking fault occurs between A and B within an ABCA cycle, the resulting cycles become ACAB [52]. Additionally, when a stacking fault is inserted between C and A, it becomes ACBC. Moreover, when a stacking fault is inserted between B and C, it becomes ACBA. This is consistent with the observed structure, as the contrast of the TEM images will be clear if this stacking fault occurs regularly in all planes. Additionally, there

Figure 7 a TEM image of the region wherein dislocations exist; b–d enlarged image of particular regions within (a).



may exist locations wherein the contrast will be unclear if the stacking fault does not occur regularly in all planes. The TEM image was comprised of both clear and unclear regions. Accordingly, these structures are attributable to stacking faults, explaining why only the one layer squeezed in between the A planes appeared to be bright. Because stacking faults are caused by partial dislocations, glide set dislocations are likely predominant. Indicated by previous studies, glide set dislocations in Si have been observed under compressive stress [21]. However, herein, many dislocations were observed for the first time in an extremely narrow area applying tensile stress in the bending test. Moreover, this study confirms the existence of stacking faults at room temperature and proposes a new mechanism for the generation of dislocations under compressive and bending stresses. The generation of dislocations caused by stacking faults has been observed in the bending of SiC nanowires with a similar crystal structure to single crystal silicon [53]. Therefore, similar phenomena are expected to occur for other materials with a diamond structure when placed under tensile stress region during a bending test.

It has been reported that single crystal silicon undergoes plastic deformation due to the activity of dislocations originating from compression or indentation tests. The mechanism of plastic deformation

under a bending stress is also thought to originate from dislocation activity. The crystal structure of single crystal silicon is a diamond structure, and the slip system which was active in this study was $\{1\ 1\ 1\}$ for the slip surface and $\langle 1\ 1\ 0 \rangle$ for the slip direction. As the load point distance of the micro-cantilever beam specimens was sufficiently larger than the height of the cross section, the applied shear stress was small and that near the top surface is regarded as pure tensile stress. At this time, the actual stress acting on the slip system (decomposition shear stress) can be calculated from the following equation:

$$\tau = \sigma m \quad (5)$$

where τ is the decomposition shear stress, σ is the tensile strength, and m is the Schmid factor (a factor related to the slip system). Herein, tensile stress was applied in the $\langle 1\ 1\ 0 \rangle$ direction and the Schmid factor in the diamond structure was $1/\sqrt{6}$ (ex. the slip surface is $\{1\ 1\ 1\}$, the slip direction is $\langle 0\ 1\ 1(-) \rangle$, the action direction of the tensile stress is $\langle 1\ 1\ 0 \rangle$). Moreover, it is possible to obtain a sufficient stress to cause a slip resulting from dislocation activity by substituting the yield stress with tensile stress in Eq. (1). The yield stress resulting in plastic deformations in both MEDIUM and SMALL specimens was within the range 4.0–4.1 GPa, all values are listed in

Table 1. Previous studies have reported the plastic deformation of single crystal Si can be obtained by dislocation in the compressive test using micropillar specimens at yield stress values of 3.0 ± 0.7 GPa [54]. The Peierls stress is estimated from the yield stress and crystal orientation. As listed in Table 1, the Peierls stress estimated from bending tests using a microcantilever beam specimens was 1.6–1.7 GPa, and that estimated from compression tests using micropillars was 1.4 GPa. These results indicate that nearly the same Peierls stresses were obtained although the specimen size and test method were different. This implies that single crystal silicon plastically deforms from the dislocation activity when under bending stress in the microscopic region at room temperature. Conversely, LARGE specimens fracture in a brittle manner without plastic deformation as their strength is lower than the yield stress.

Observed by TEM, dislocations were unevenly distributed within a specific range of the tensile surface. To investigate the validity of the plastic deformation area size, area size was compared with calculated results derived under the assumption that the tensile stress acts linearly through the neutral plane to the tensile plane in the microcantilever beam specimens. Additionally, assuming that the dislocations are generated within a region where the applied stress was equal to or larger than the yield stress, the size of the plastic deformation area can be calculated by:

$$L = \frac{(\sigma_{\max} - \sigma_{\tau})a}{\sigma_{\max}} \tag{6}$$

where L is the size of the region where the tensile stress larger than the yield stress, a is the distance from the neutral plane to the tensile plane, σ_{\max} is the applied maximum tensile stress, and σ_{τ} is the yield stress. As the specimen observed by TEM was sampled from the center of the microcantilever beam specimen with a pentagonal cross section, the distance from the neutral plane (a) was $1.1 \mu\text{m}$ in the MEDIUM specimen; the yield stress (σ_{τ}) was 4 GPa as listed in Table 1, and the maximum tensile stress (σ_a) was 7.0 GPa. The size of the plastic deformation region, as calculated from these values, was 475 nm and approximately agrees with the size of the plastic deformation region observed in the TEM image. Based on the above considerations, it can be said that the size of the plastic deformation region observed by TEM is reasonable.

Size effect of strength in microscopic region of single crystal silicon

The relationship between the bending strength of variously sized specimens was obtained using the microcantilever method; the volume calculated from the cross-sectional area of the specimen and the distance from the specimen’s end to the loading point are shown in Fig. 8. The bending strength was plotted against the total volume as specimens in this study were nearly homothetic, though the effective volume should be used in the Weibull statistic. The bending strengths of the microcantilever beam specimens were 4.1 ± 0.4 , 9.0 ± 1.4 , and 14.2 ± 1.4 GPa for the LARGE, MEDIUM, and SMALL specimens, respectively; note that these values increased with decreasing specimen size. A similar increase in strength with decreasing specimen size has also been reported for bulk brittle solids; we confirm that a microcantilever beam specimen of several micrometer can exhibit size effects with regard to the bending strength. In particular, the strength of the SMALL specimen was 14.2 GPa, an extremely high value. As this value is very close to the ideal strength required for cutting bonds between the Si atoms through first-principle calculation [55], it was confirmed that size effects are present in the bending strength of such a microscopic region. Generally, the size effect acting on the bending strength likely originates from the existence of coarse defects in the specimens; this would result in the observed strength increase with a decrease in the specimen size. Assuming that linear elastic fracture mechanics apply in a microscopic

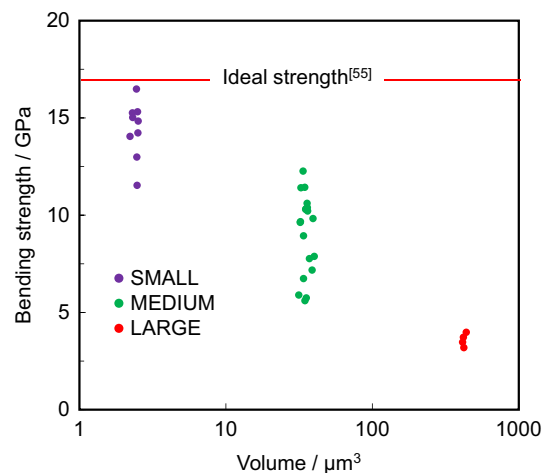


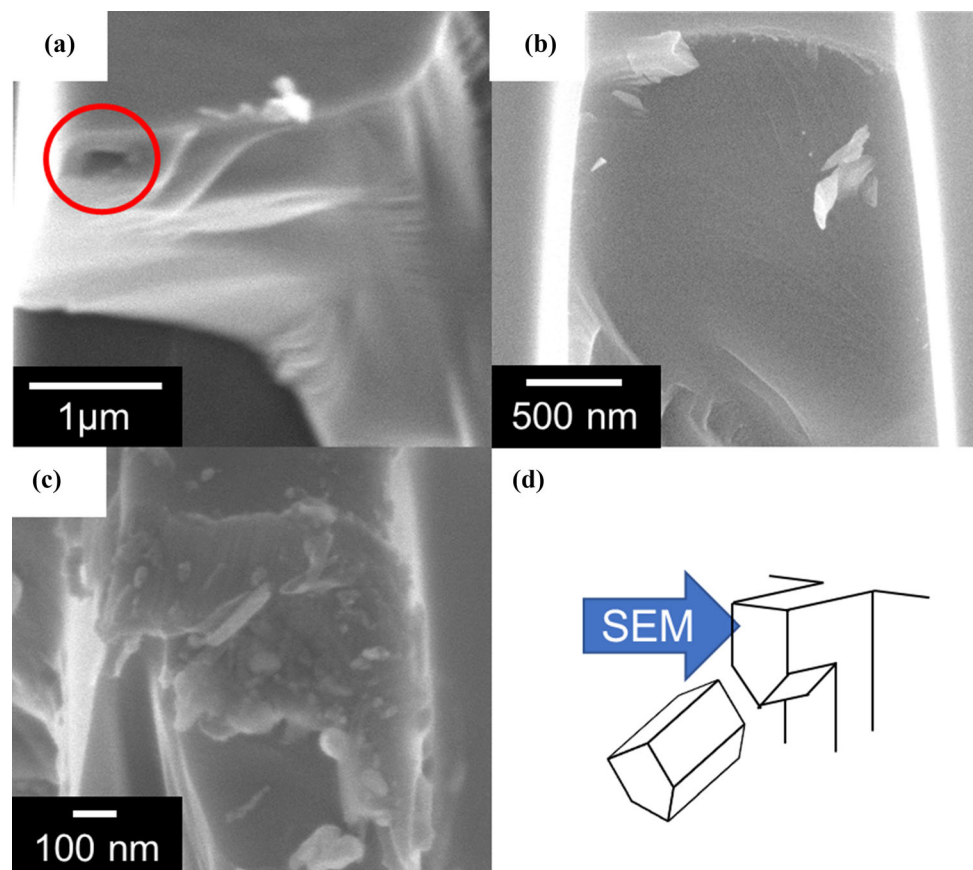
Figure 8 Relationship between bending stress and volume for each microcantilever beam specimen with different sizes.

region, the crack length obtained from bending strength measurements was calculated using the Griffith equation and the fracture toughness, K_{IC} . The fracture toughness of the single crystal silicon was $1.05 \text{ MPam}^{1/2}$ when measured using microcantilever beam specimens. This value is similar to those reported in the previous studies [29, 43, 56–61]. Herein, two types of cracks were assumed as the shape of defects, these being a stress through crack and a penny-shaped crack in infinite body; this second crack type is used to estimate the size of fracture origin because it is difficult to estimate the geometry of the accumulation region of dislocations. The crack lengths calculated using the shape factor Y of the assumed crack geometry are listed in Table 1. Fractography was carried out to confirm these defects. The fracture surface of the microcantilever beam specimens was observed via field emission SEM (FE-SEM). As presented in Fig. 9, for the LARGE specimen, several hundreds of nanometers of fracture's origin could be confirmed. On the other hand, the fracture origin for both the MEDIUM and SMALL specimens could not be clearly observed.

Considering the estimated crack length, there is a possibility that the fracture origins could not be observed with FE-SEM as these samples were extremely small, in the range of several nanometers.

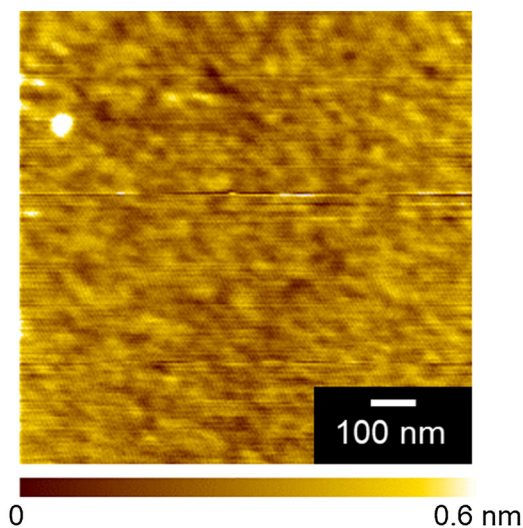
As silicon has a higher yield stress than metals such as copper, the plastic strain gradient has little effect on the size effect [62]. However, the stress gradient greatly affects the size effect as the microcantilever method is technically a bending test. The crack lengths present in the SMALL specimen were smaller than those formed in the MEDIUM specimen; this is due to the stress gradient in the specimen during the bending test. Microcantilever beam specimen undergoing the bending test displays a stress grading of tensile stress from the neutral surface through to the surface of the specimen. When the same stress is applied to the specimen, the slope of the stress gradient is large because a SMALL specimen has a shorter distance from the neutral surface to the surface of the specimen. The range in which sufficient stress to generate and accumulate the dislocations is narrowed, so the range in which

Figure 9 SEM images of fracture surfaces: **a** LARGE, **b** MEDIUM, **c** SMALL, and **d** direction of view.



dislocations accumulate in SMALL specimens is smaller than that of the MEDIUM specimen.

It has been previously reported that the fracture origin in small single crystal silicon is caused by surface roughness of the specimen [33]. Figure 10 shows the SPM image of a single crystal silicon surface onto which microcantilever beam specimens were prepared. The surface of the chemically mechanically polished silicon substrate was very flat, displaying a maximum height roughness of 0.33 nm; the maximum high roughness is defined as the difference between the peak and the valley in 1 μm square surface profile. In this previous study, it was reported that the roughness of the chemically mechanically polished surface of single crystal silicon was 0.135 nm [63], similar to yet smaller than that measured in this study. This is suggestive that both the MEDIUM and SMALL specimens did not fracture from the fracture origin, owing to the surface roughness of the substrate. According to fracture mechanics theory, the stress concentrates in the region wherein dislocations aggregate like cracks [64]; this region of accumulated dislocations may be the fracture origin for brittle solids. As shown in Fig. 6c, there exists an origin where the dislocations accumulated with high density in the vicinity of the fixed end of the beam, where a large tensile stress acted; the size was approximately 15 nm. This value



Calculated average roughness: 0.05 nm
Maximum height roughness : 0.33 nm

Figure 10 SPM surface image of a single crystal silicon onto which microcantilever beam specimens were prepared.

is within the range of 10.3–25.3 nm; this being the estimated range for crack lengths for the MEDIUM specimen under the assumption that all crack geometries conform to straight through crack and penny-shaped crack models, respectively, results presented in Table 1. As the specimen observed by TEM did not undergo stress until fracturing, the size of the dislocation accumulation area observed by TEM and the crack length calculated using the Griffith equation are in good agreement. Thus, the fracture origin for a microcantilever beam specimen should be the region of concentrated stress caused by the accumulation of dislocations. Stated otherwise, we have shown that the bending strength of the microscopic region within a micrometer-scale single crystal silicon exhibits a size effect controlled primarily by the accumulation of dislocations, unlike the case of a bulk solid. Although the region of accumulated dislocations was not observed in the SMALL specimen, it should be smaller than that within the MEDIUM specimen; this size difference is due to the steeper stress distribution in the bending test of the microcantilever beam specimen. As a result, it seems that the strength of the SMALL specimen was higher than that of the MEDIUM specimen because the dense dislocation region is smaller in the smaller size specimen.

As described above, the single crystal silicon in a microscopic region of several μm fractured by a defect resulting from the accumulation of dislocations. Generally, the strength of brittle solids is typically discussed in terms of an existing defect within the material. However, the observations reported herein indicate that it is also necessary to consider the generation of defects in materials with a microstructure. This new consideration—regarding dislocation-controlled microscopic mechanical phenomena under bending stress at room temperature—provides an understanding of the mechanism of the mechanism by which defects are generated and cracks propagate resulting in fatigue or wear of, not only microelectromechanical systems devices and silicon nanowires, but also all materials.

Conclusion

Herein, the mechanical properties of single crystal silicon were evaluated using microcantilever beam specimens of various sizes. We found novel

microscopic mechanical phenomena which are controlled by dislocations in single crystal silicon when undergoing bending stress at room temperature. Young's modulus estimated from the initial stage of the stress–strain curve of the microcantilever beam specimens showed a similar value to that resulting from the first-principle calculation. Smaller specimens displayed nonlinear deformation under high bending stress. TEM observations clearly indicate that the deformation resulted from the formation and movement of dislocations. The bending strength increased as the volume of the specimen decreased, while the smallest specimens displayed nearly ideal strength. The accumulation of dislocations in smaller specimens was found to be nanoscale in size, observed by TEM observation. Furthermore, it was shown that the extent of regional localization of where dislocations accumulated dominated the bending strength of the single crystal silicon microcantilever beam specimens as a newly generated defect. Consequently, bending tests using microcantilever beam specimens and their TEM observation revealed novel dislocation-controlled microscopic mechanical phenomena in single crystal silicon under bending stress at room temperature.

Acknowledgements

This work was partly supported by JSPS KAKENHI Grant Numbers 17H01319.

Electronic supplementary material: The online version of this article (<https://doi.org/10.1007/s10853-020-04528-3>) contains supplementary material, which is available to authorized users.

References

- [1] Chen W, Liu Y, Wu J, Chen Q, Zhao Y, Wang Y, Du X (2019) High-efficient solar cells textured by Cu/Ag-cocatalyzed chemical etching on diamond wire sawing multicrystalline silicon. *ACS Appl Mater Interfaces* 11:10052–10058
- [2] Xu ZL, Liu X, Luo Y, Zhou L, Kim JK (2017) Nanosilicon anodes for high performance rechargeable batteries. *Prog Mater Sci* 90:1–44
- [3] Harpak N, Davidi G, Schneier D, Menkin S, Mados E, Golodnitsky D, Peled E, Patolsky F (2019) Large-scale self-catalyzed spongelike silicon nano-network-based 3D anodes for high-capacity lithium-ion batteries. *Nano Lett* 19:1944–1954
- [4] Pandolfi S, Lecuna CR, Godec YL, Baptiste B, Menguy N, Lazzeri M, Gervais C, Spektor K, Crichton WA, Kurakevych OO (2018) Nature of hexagonal silicon forming via high-pressure synthesis: nanostructured hexagonal 4H polytype. *Nano Lett* 18:5989–5995
- [5] Asano K, Tang H, Chen CY, Nagoshi T, Chang TFM, Yamane D, Konishi T, Machida K, Masu K, Sone M (2018) Promoted bending strength in micro-cantilevers composed of nanograined gold toward MEMS applications. *Microel Eng* 196:20–24
- [6] Tang H, Hashigata K, Chang TFM, Chen CY, Nagoshi T, Yamane D, Konishi T, Machida K, Masu K, Sone M (2018) Sample size effect on micro-mechanical properties of gold electroplated with dense carbon dioxide. *Surf Coat Technol* 350:1065–1070
- [7] Dehm G, Jaya BN, Raghavan R, Kirchlechner C (2018) Overview on micro- and nanomechanical testing: new insights in interface plasticity and fracture at small length scales. *Acta Mater* 142:248–282
- [8] Ramezany A, Pourkamali S (2018) Ultrahigh frequency nanomechanical piezoresistive amplifiers for direct channel-selective receiver front-ends. *Nano Lett* 18:2551–2556
- [9] Lu YW, Shieh J, Tsai FY (2016) Induction of ferroelectricity in nanoscale ZrO₂/HfO₂ bilayer thin films on Pt/Ti/SiO₂/Si substrates. *Acta Mater* 115:68–75
- [10] Schlich FF, Spolenak R (2016) Size- and phase-dependent mechanical properties of ultrathin Si films on polyimide substrates. *Acta Mater* 110:122–130
- [11] Cook RF (2006) Strength and sharp contact fracture of silicon. *J Mater Sci* 41:841–872. <https://doi.org/10.1007/s10853-006-6567-y>
- [12] Jadaan OM, Nemeth NN, Bagdahn J, Sharpe WN Jr (2003) Probabilistic Weibull behavior and mechanical properties of MEMS brittle materials. *J Mater Sci* 38:4087–4113. <https://doi.org/10.1023/A:1026317303377>
- [13] Hauch JA, Holland D, Marder MP, Swinney HL (1999) Dynamic fracture in single crystal silicon. *Phys Rev Lett* 82(19):2823–2826
- [14] Lawn B (1975) *Fracture in brittle solids*. Cambridge University Press, Cambridge
- [15] Mier JGMV, Vliet MRAV (2003) Influence of microstructure of concrete on size/scale effects in tensile fracture. *Eng Fract Mech* 70:2281–2306
- [16] Östlund F, Malyska KR, Leifer K, Hale L, Tang Y, Ballarini R, Gerberich W, Michler J (2009) Brittle-to-ductile transition

- in uniaxial compression of silicon pillars at room temperature. *Adv Funct Mater* 19:2439–2444
- [17] Wang YC, Zhang W, Wang LY, Zhuang Z, Ma E, Li J, Shan ZW (2016) In situ TEM study of deformation-induced crystalline-to-amorphous transition in silicon. *NPG Asia Mater* 8:e291
- [18] Wessel K, Alexander H (1977) On the mobility of partial dislocations in silicon. *Philos Mag* 35(6):1523–1536
- [19] Nishino Y, Saka H, Imura T (1984) Temperature dependence of friction force acting on dislocations in silicon crystals. *J Mater Sci* 19:245–253. <https://doi.org/10.1007/BF02403131>
- [20] Izumi S, Ohta H, Takahashi C, Suzuki T, Saka H (2010) Shuffle-set dislocation nucleation in semiconductor silicon device. *Philos Mag Lett* 90(10):707–714
- [21] Castaing J, Veyssiere P, Kubin L, Rabier J (1981) The plastic deformation of silicon between 300 and 600 °C. *Philos Mag* 44(6):1407–1413
- [22] Okuno T, Saka H (2013) Electron microscope study of dislocations introduced by deformation in a Si between 77 and 873 K. *J Mater Sci* 48:115–124. <https://doi.org/10.1007/s10853-012-6860-x>
- [23] Asaoka K, Umeda T, Arai S, Saka H (2005) Direct evidence for shuffle dislocations in Si activated by indentations at 77K. *Mater Sci Eng A* 400–401:93–96
- [24] Ray I, Cockayne D (1971) The dissociation of dislocations in silicon. *Proc R Soc A* 325:543–554
- [25] Rabier J (2007) High-stress plasticity and the core structures of dislocations in silicon. *Phys Stat Sol* 204(7):2248–2255
- [26] Saka H, Yamamoto Y, Arai S, Kuroda K (2006) In-situ TEM observation of transformation of dislocations from shuffle to glide sets in Si under supersaturation of interstitials. *Philos Mag* 86:4841–4850
- [27] William WG, Douglas DS, Aaron RB, Natalia IT (2011) A brittleness transition in silicon due to scale. *J Mater Res* 27(3):552–561
- [28] Elhebeary M, Saif MTA (2018) A novel MEMS stage for in situ thermomechanical testing of single crystal silicon microbeams under bending. *Extreme Mech Lett* 23:1–8
- [29] Balila NJ, Jeffrey MW, Juri W, James PB, Rafael S, Johann M, Christoph K, Gerhard D (2016) Microscale fracture behavior of single crystal silicon beams at elevated temperatures. *Nano Lett* 16:7597–7603
- [30] Wang B, Zhang Z, Chang K, Cui J, Rosenkranz A, Yu J, Lin CT, Chen G, Zang K, Luo J, Jiang N, Guo D (2018) New deformation-induced nanostructure in silicon. *Nano Lett* 18:4611–4617
- [31] Tsuchiya T, Hemmi T, Suzuki J, Hirai Y, Tabata O (2018) Tensile strength of silicon nanowires batch-fabricated into electrostatic MEMS testing device. *Appl Sci* 8:880
- [32] Fugii T, Sudoh K, Inoue S, Namazu T (2016) Design and development of electrostatically driven uniaxial tensile test device for silicon nanowires. *Sens Mater* 28(2):89–102
- [33] Sundararajan S, Bhushan B (2002) Development of AFM-based technique to measure mechanical properties of nanoscale structures. *Sens Actuat A* 101:338–351
- [34] Sundararajan S, Bhushan B, Namazu T, Isono Y (2002) Mechanical property measurements of nanoscale structures using an atomic force microscope. *Sens Actuat A* 91:111–118
- [35] Fujii T, Sudoh K, Sakakihara S, Naito M, Inoue S, Namazu T (2013) Nano-scale tensile testing and sample preparation techniques for silicon nanowires. *Jpn J Appl Phys* 52:110118
- [36] Kang W, Saif MTA (2013) In situ study of size and temperature dependent brittle-to-ductile transition in single crystal silicon. *Adv Funct Mater* 23:713–719
- [37] Tsuchiya T, Hemmi T, Suzuki J, Hirai Y, Tabata O (2016) Tensile fracture of integrated single-crystal silicon nanowire using MEMS electrostatic testing device. *Proc Struct Integr* 2:1405–1412
- [38] Goel S, Kovalchenko A, Stukowski A, Cross G (2016) Influence of microstructure on the cutting behaviour of silicon. *Acta Mater* 105:464–478
- [39] Tang DM, Ren CL, Wang MS, Wei X, Kawamoto N, Liu C, Bando Y, Mitome M, Fukata N, Golberg D (2012) Mechanical properties of Si nanowires as revealed by in situ transmission electron microscopy and molecular dynamics simulations. *Nano Lett* 12:1898–1904
- [40] Wang L, Zheng K, Zhang Z, Han X (2011) Direct atomic-scale imaging about the mechanisms of ultralarge bent straining in Si nanowires. *Nano Lett* 11:2382–2385
- [41] Uesugi A, Hirai Y, Tsuchiya T, Tabata O (2016) Effect of crystallographic orientations on fractures and slip occurrences at 500 °C of (110) single crystal silicon microstructures. *Proc Struct Integr* 2:1413–1420
- [42] Fujita S, Tatami J, Yahagi T, Takahashi T, Iijima M (2017) Degradation evaluation of Si₃N₄ ceramic surface layer in contact with molten Al using microcantilever beam specimens. *J Eur Ceram Soc* 37:4351–4356
- [43] Tatami J, Katayama M, Ohnishi M, Yahagi T, Takahashi T, Horiuchi T, Yokouchi M, Yasuda K, Kim DK, Wakihara T, Komeya K (2015) Local fracture toughness of Si₃N₄ ceramics measured using single-edge notched microcantilever beam specimens. *J Am Ceram Soc* 98(3):965–971
- [44] Camposivan E, Anglada M (2016) Size and plasticity effects in zirconia micropillars compression. *Acta Mater* 103:882–892
- [45] Wheeler JM, Raghavan R, Wehrs J, Zhang Y, Erni R, Michler J (2016) Approaching the limits of strength:

- measuring the uniaxial compressive strength of diamond at small scales. *Nano Lett* 16:812–816
- [46] Lu Y, Shu X, Liao X (2018) Size effect for achieving high mechanical performance body-centered cubic metals and alloys. *Sci China Mater* 61(12):1495–1516
- [47] Yamaguchi H, Tatami J, Iijima M (2019) Measurement of mechanical properties of BaTiO₃ layer in multilayered ceramic capacitor using a microcantilever beam specimen. *J Ceram Soc Jpn* 127(6):335–338
- [48] Colas G, Serles P, Saulot A, Filleter T (2019) Strength measurement and rupture mechanisms of a micron thick nanocrystalline MoS₂ coating using AFM based micro-bending test. *J Mech Phys Solids* 128:151–161
- [49] Yoshida K, Nishiyama N, Sone M, Wakai F (2017) Strength and toughness of nanocrystalline SiO₂ stishovite toughened by fracture-induced amorphization. *Acta Mater* 124:316–324
- [50] Ronan H, Thierry B, Thierry D, Armel DM, Isabelle ZA, Jean MG, Cyril L, Sylvain M (2019) Local fracture toughness measurements in polycrystalline cubic zirconia using micro-cantilever bending tests. *Mech Mater* 136:103086
- [51] Brantley WA (1973) Calculated elastic constants for stress problems associated with semiconductor devices. *J Appl Phys* 44(1):534–535
- [52] Saka H (2017) *Classical theory of crystal dislocations: from iron to gallium nitride*. World Scientific, Singapore
- [53] Han XD, Zhang YF, Zheng K, Zhang XN, Zhang Z, Hao YJ, Guo XY, Yuan J, Wang ZL (2007) Low-temperature in situ large strain plasticity of ceramic SiC nanowires and its atomic-scale mechanism. *Nano Lett* 7(2):452–457
- [54] Rabier J, Renault PO, Eyidi D, Demenet JL, Chen J, Couvy H, Wang L (2007) Low-temperature in situ large strain plasticity of ceramic SiC nanowires and its atomic-scale mechanism. *Phys Stat Sol C* 4:3110
- [55] Dubois SMM, Rignanese GM, Pardo T, Charlier JC (2006) Ideal strength of silicon: an ab initio study. *Phys Rev B* 74:235203
- [56] Sumigawa T, Ashida S, Tanaka S, Sanada K, Kitamura T (2015) Fracture toughness of silicon in nanometer-scale singular stress field. *Eng Fract Mech* 150:161–167
- [57] Gallo P, Yan Y, Sumigawa T, Kitamura T (2018) Fracture behavior of nanoscale notched silicon beams investigated by the theory of critical distances. *Adv Theory Simul* 1:1700006
- [58] Gallo P, Sumigawa T, Kitamura T (2019) Experimental characterization at nanoscale of single crystal silicon fracture toughness. *Frattura ed Integrità Strutturale* 47:408–415
- [59] Kunio H, Shinji T, Yasunori O, Tomozo N (1991) Fracture toughness of single crystal silicon. *J Soc Mater Sci Jpn* 40(451):405–410
- [60] Balila NJ, Christoph K, Gerhard D (2014) Can microscale fracture tests provide reliable fracture toughness values? A case study in silicon. *J Mater Res* 30(5):686–698
- [61] Ando T, Li X, Nakano S, Kasai T, Tanaka H, Shikida M, Sato K (2005) Fracture toughness measurement of thin film silicon. *Fatigue Fract Eng Mater Struct* 28:687–694
- [62] Motz C, Schöberl T, Pippin R (2005) Mechanical properties of micro-sized copper bending beams machined by the focused ion beam technique. *Acta Mater* 53:4269–4279
- [63] Jiang BC, Zhao DW, Wang BQ, Zhao HJ, Liu YH, Lu XC (2019) Flatness maintenance and roughness reduction of silicon mirror in chemical mechanical polishing process. *Sci China Technol Sci*. <https://doi.org/10.1007/s11431-018-9414-6>
- [64] Johannes W (1996) *Dislocation based fracture mechanics*. World Scientific, Singapore

Publisher's Note Springer Nature remains neutral with regard to jurisdictional claims in published maps and institutional affiliations.